



HAL
open science

Numerical simulation of metal forming processes with 3D adaptive Remeshing strategy based on a posteriori error estimation

Bessam Zeramdini, Camille Robert, Guenaël Germain, Thomas Pottier

► **To cite this version:**

Bessam Zeramdini, Camille Robert, Guenaël Germain, Thomas Pottier. Numerical simulation of metal forming processes with 3D adaptive Remeshing strategy based on a posteriori error estimation. *International Journal of Material Forming*, 2019, 12 (3), pp.411-428. 10.1007/s12289-018-1425-4 . hal-01881339

HAL Id: hal-01881339

<https://imt-mines-albi.hal.science/hal-01881339>

Submitted on 4 Dec 2018

HAL is a multi-disciplinary open access archive for the deposit and dissemination of scientific research documents, whether they are published or not. The documents may come from teaching and research institutions in France or abroad, or from public or private research centers.

L'archive ouverte pluridisciplinaire **HAL**, est destinée au dépôt et à la diffusion de documents scientifiques de niveau recherche, publiés ou non, émanant des établissements d'enseignement et de recherche français ou étrangers, des laboratoires publics ou privés.

Numerical simulation of metal forming processes with 3D adaptive Remeshing strategy based on a posteriori error estimation

Bessam Zeramdini¹ · Camille Robert¹ · Guenael Germain¹ · Thomas Pottier²

Abstract

In this work, a fully automated adaptive remeshing strategy, based on a tetrahedral element for 3D metal forming processes, was proposed in order to solve problems associated with the severe mesh distortion that occurs during the computation. The main idea is to use the h-type adaptive mesh in combination with an a-posteriori error estimator measured (by the energy norm) on each finite elements to locally control the mesh modification-as-needed. Once a new mesh is generated, all history-dependent variables must be carefully transferred between subsequent meshes. Therefore, several transfer techniques are described and compared. A special attention is given to restore the local mechanical equilibrium of the system with a new methodology. After presenting the necessary adaptive remeshing steps, some 3D analytic and numerical results using the proposed adaptive strategy are given to demonstrate the capabilities of the proposed equilibrated approach and to illustrate some practical characteristics of our remeshing process.

Keywords 3D metal forming processes · Automatic adaptive remeshing · A-posteriori error estimator · Transfer techniques · Equilibrated process

Introduction

For a large class of problems such as metal forming process like forging, rolling, cutting, etc., the use of the finite element method is still a challenging problem. It can typically involve high strain localization, large inelastic deformations and high

temperature problems. Often in these types of application, mesh becomes unacceptable due to severe distortion or complex workpiece-die contact occurring which induces errors in the key internal variables (plastic strains and stresses). As consequence, the ability to achieve a proper analysis with reasonable CPU cost is entirely dependent on the FE mesh spacing. Indeed, optimal mesh configuration changes continuously throughout the metal forming process. Consequently, the final results obtained with the use of a fixed mesh are unreliable and may give a rise to severe numerical difficulties and may even make it impossible to pursue the calculations any further because of severe element distortion. In order to overcome these difficulties and continue the simulation for large deformation cases, successive mesh adaptation is needed during the numerical simulation in order to obtain an optimal discretization according to the geometrical shape or/and physical solution. The main ingredients in any adaptive procedure are a posteriori error estimation and a mesh generator [1]:

-
- Adaptive mesh strategy is developed for 3D metal material processes.
 - Different methods recovery techniques are compared.
 - Equilibrium method for dynamic explicit scheme is proposed.
 - Results are compared with experiments test.
-

✉ Bessam Zeramdini
bessam.zeramdini@ensam.eu

Camille Robert
camille.robert@ensam.eu

Guenael Germain
guenael.germain@ensam.euand

Thomas Pottier
thomas.pottier@mines-albi.fr

¹ LAMPA, Arts et Métiers, 2 Boulevard du Ronceray, 49000 Angers, France

² Institut Clement Ader, Ecole Nationale Supérieure des Mines d'Albi Mines d'Albi-Carmaux, Campus Jarlard, 81013 Albi, France

- (i) The a posteriori error estimation is required to decide if the previous FEM calculation must be stopped, to locate the critical zones of the domain where the mesh need to be concentrated or to be coarsened and to determine the size of optimal mesh. An overview of different a posteriori error estimation technique is provided by [2, 3].

- (ii) The mesh generator produces the new spatial discretization with the desired element density at prescribed locations in the deformed configuration, as determined after the error assessment. While the spatial discretization changes between subsequent mesh, the global topology of the piece is conserved. In the approach presented here, unstructured tetrahedral elements with local h-adaptive strategy guided by error indicators and geometric approximation are used. The advantages of their use are discussed by Lo [4, 5].

Once a new mesh is generated, two approaches are possible: either the simulation is totally recomputed, or all the state variables and history-dependent variables at the end of the previous load step must be transferred from the degenerated old mesh to the reconstructed new one, in order to continue the simulation. Owing to the fact that the optimal mesh configuration and the boundary conditions changes continuously throughout the numerical simulation, the second approach will be implemented step by step in order to adapt to this change. This is a delicate issue because if the new field variables are not adequately determined, the simulation accuracy can be severely affected [6]. Different techniques exist to transfer the history variables; basically all these methods can be categorized into two types: direct transfer (closest point technique [7], weighted average method [8], Superconvergent recovery by element patches [9], etc.), and indirect transfer (such as least squares smoothing, average values [10], the superconvergent patch recovery (SPR) technique [11–13], etc.).

In the present paper, after a concise review of error estimation and the alternative mesh refinement criteria in Section “[Error estimators](#)”, different Patch Recovery Techniques such as average values technique (Avg), superconvergent patch recovery (SPR) and the modified of Zienkiewicz and Zhu technique (SPR-P) will be described in Section “[Patch recovery techniques](#)”. Then in Section “[Analytical results](#)” these recovery methods will be compared with analytics function in order to select the best techniques to transfer the data state variables between two successive meshes. In Section “[Adaptive remeshing methodology](#)”, the global flowchart of the proposed 3D adaptive remeshing algorithm is detailed. In Section “[Numerical results](#)”, the efficiency of algorithm here proposed and the equilibrated approach are validated through various examples including the shear test as well as the forging process. Finally some conclusions are drawn in Section “[Conclusion](#)”.

Error estimators

The error estimation is the first and one of the most important procedures in adaptive FE analysis. Because it indicates the quality of elements, quality of the solution, and if necessary

new element density. Among the very numerous proposals that were, and still are available, three groups can be classified, depending on whether they are based on: the estimators based on residuals analysis, introduced by Babuska and Rheinboldt [14], the estimators based on the concept of error in constitutive relation, initiated by Ladvéze et al. [15], and the estimators based on smoothing techniques developed by Zienkiewicz et Zhu [16]. Although the approach of the residual estimator proposed by Babuška and Rheinboldt [14] is mathematically rigorous, its extension to 3D nonlinear problems is facing some major challenges. Indeed the efficiency of this estimator depends on the mesh quality and regularity of the solution, which makes it less suitable for large deformation problems. In the literature, the majority of applications are presented in the context of 1D and 2D academic problems. The key point of the proposed estimator by Ladevèze et al. [15] is the construction of admissible displacement-stress pair. For the sake of simplicity, in the context of FE method with compressible material, the displacement field can be considered as admissible. Conversely, the stress field is not statically admissible. In the literature, Sever method can be used to calculate this admissible stress [17]. In spite of its remarkable efficiency, this technique has been rarely used in FE simulation software because of the cost of its implementation. In this work, the estimator based on smoothing techniques is used due to its cost effectiveness and reliability to estimate errors and for its simplicity of implementation. The main idea of the smoothing techniques is based on the construction of a recovered stress tensor field $\tilde{\sigma}$ more accurate than the finite element solution σ_h . This recovered stress tensor field $\tilde{\sigma}$, can be constructed by a variety of projection techniques, such as: least squares smoothing, average values, the superconvergent patch recovery (SPR) technique etc..

In the following part, the average values technique, the SPR error estimator in its almost standard form and the modified Zienkiewicz and Zhu technique (SPR-P), will be studied.

A posteriori error estimation

We suppose that the FE solution (u_h, σ_h) is an approximation of the exact solution θ_{imp} in the considered finite element space Ω . The displacement error e^u is the difference between the exact displacement solution and the FE displacement solution:

$$e^u = u - u_h \quad (1)$$

The stress error e^σ is the difference between the exact stress field and the FE stress field:

$$e^\sigma = \sigma - \sigma_h \quad (2)$$

Dealing with problems of metal forming process and mechanical structure, the element error is generally given, according to the norm of energy [18, 19]. It expresses the difference between the exact stress σ and the FE one σ_h :

$$\|e^\sigma\|_{el} = \|\sigma - \sigma_h\|_{el} = \left(\int_{\Omega} (\sigma - \sigma_h) : (\varepsilon - \varepsilon_h) d\omega \right)^{1/2} \quad (3)$$

To evaluate the quality of the approximate error norm it is more logical to use a relative value, given as:

$$\theta_{el} = \frac{e^\sigma_{el}}{\left(\int_{\Omega} \sigma : \varepsilon d\omega \right)^{1/2}} \quad (4)$$

Practically, it is not possible to compute the exact error e^σ . The exact solutions (σ, ε) are further approximated by smoothed stress distribution Ones $(\tilde{\sigma}, \tilde{\varepsilon})$, which are computed from the FE solutions using Patch Recovery Techniques presented thereafter. Therefore, the stress error modelling is given by:

$$e^{\tilde{\sigma}} = \tilde{\sigma} - \sigma_h \quad (5)$$

Dealing with problems of metal forming process and mechanical structure, the element error norm will be defined by:

$$\|e^{\tilde{\sigma}}\|_{el} = \|\tilde{\sigma} - \sigma_h\|_{el} = \left(\int_{\Omega} (\tilde{\sigma} - \sigma_h) : (\tilde{\varepsilon} - \varepsilon_h) d\omega \right)^{1/2} \quad (6)$$

Then, the global error $\tilde{\theta}$ over the whole structure Ω is calculated by summing the errors of all the elements.

$$\|e^{\tilde{\sigma}}\|_{\Omega}^2 = \sum_{el \in \Omega} \|e^{\tilde{\sigma}}\|_{el}^2 \quad (7)$$

$$\tilde{\theta} = \left(\sum_{el \in \Omega} (\tilde{\theta}_{el})^2 \right)^{1/2} \quad (8)$$

$$\tilde{\theta}_{el} = \frac{\|e^{\tilde{\sigma}}\|_{el}}{\left(\int_{\Omega} \tilde{\sigma} : \tilde{\varepsilon} d\omega \right)^{1/2}} \quad (9)$$

The dependability of the estimate is measured by its effectivity index ξ defined, in each element of the mesh, as the ratio between the predicted error and the exact error as measured respectively in Eq. (6) and expression Eq. (3). Thus:

$$\xi = \frac{\|e^{\tilde{\sigma}}\|_{el}}{\|e^\sigma\|_{el}} \quad (10)$$

An error estimator is considered as asymptotically exact when its efficiency index tends to 1, in other words when the size of items tends to zero [2, 9, 12, 19].

Size map for adaptive strategies

After estimating the element error, an establishment of a relation between this error and the element size is needed afterwards. Usually, this relation can be established with the using either of the following two strategies: The first allows us to calculate an optimal mesh for a prescribed accuracy, while the second seeks to optimize a mesh under the constraint of a number of degrees of freedom attached. One may refer to [18, 19] for more details, which used a combination of them. The first strategy is used to compute an optimized new mesh. Then, if the number of elements exceeds the prescribed number of degrees of freedom the new mesh will be computed with the second strategy. Many others authors [20] propose other similar optimization strategies that aim to control the size of the problem studied. They seek maximum accuracy to reach for a fixed size memory or CPU time for a given calculation. In the present work, only the first strategy will be studied because the goal of this paper is to evenly distribute the error over all the elements.

Optimal mesh for prescribed accuracy θ^{imp} :

According to finite element convergence theorem, the local element error is directly related to its characteristic length h_{el} and its rate of convergence p . In three-dimensional case, p is equal to 1 for the linear tetrahedron element [21].

$$\tilde{\theta}_{el} = O(h_{el}^p) \quad (11)$$

Assuming that the rate of convergence of the FEM is uniform throughout the entire domain Ω , the optimal size of each element must be computed by:

$$\frac{\tilde{\theta}_{el}^{opt}}{\tilde{\theta}_{el}} = \left(\frac{h_{el}^{opt}}{h_{el}} \right)^p, \quad (12)$$

Where h_{el} and h_{el}^{opt} denote respectively the current characteristic size of an element el and the optimal characteristic size of the new one. $\tilde{\theta}_{el}$ and $\tilde{\theta}_{el}^{opt}$ represent the predicted and optimal element error to the current mesh and the optimal one, respectively.

$$\tilde{\theta} = \left(\sum_{el \in \Omega} (\tilde{\theta}_{el})^2 \right)^{1/2} \quad (13)$$

$$\theta^{imp} = \left(\sum_{el \in \Omega} (\tilde{\theta}_{el}^{opt})^2 \right)^{1/2} \quad (14)$$

In three-dimensional case, the optimal number of elements is given by [19]:

$$nelt^{opt} = \sum_{el} \left(\frac{h_{el}^{opt}}{h_{el}} \right)^{-d}, \quad (15)$$

where $nelt$ is the total number of elements within the domain Ω and d is the number of degrees of freedom.

The optimality condition of the expected mesh leads to uniform the error θ^{umi} on the new elements, which gives:

$$\forall el, \left(\tilde{\theta}_{el}^{opt} \right)^2 = (\theta^{umi})^2 \left(\frac{h_{el}^{opt}}{h_{el}} \right)^{-d} \quad (16)$$

From Eqs. (14) and (16), the target error θ^{inp} accepted by the user is given by:

$$(\theta^{inp})^2 = (\theta^{umi})^2 \sum_{el}^{nelt} \left(\frac{h_{el}^{opt}}{h_{el}} \right)^{-d}, \quad (17)$$

then, a new element size factor can be computed from Eqs. (12) and (16).

$$\frac{h_{el}^{opt}}{h_{el}} = \left(\frac{\theta^{umi}}{\tilde{\theta}_{el}} \right)^{2/(2p+d)} \quad (18)$$

The final expression of the resize coefficient is written as a function of the estimated error, the target error and the convergence rate p :

$$\frac{h_{el}^{opt}}{h_{el}} = \frac{(\theta^{inp})^{1/p}}{\left(\tilde{\theta}_{el} \right)^{2/(2p+d)} \left(\sum_{el}^{nelt} \left(\tilde{\theta}_{el} \right)^{2d/(2p+d)} \right)^{1/2p}} \quad (19)$$

Patch recovery techniques

The transferring approach strongly depends on the kind of state variables which needs to be transferred [22]. At least, when transferring the nodal variables (such as displacements, velocity and temperature) a direct interpolation from old nodes to the new ones may be used via the finite element shape function. However, the transfer of the element variables (such as stress, strain and internal variables) is a very difficult problem. This problem has been addressed by many authors [10, 22].

Here, the nodal displacement data is already present in the updated geometry of the problem because the remeshing strategy is done in the deformed configuration. In fact, only integration point variables need to be transferred. It should also be noted that in the case of a thermo-dynamic test, also the temperature must be transferred from the old node to the new ones. In order to study the compatibility of the element state transfer with the initial field and the numerical diffusion solution, numerical result using three recovery methods will be compared in the next part with analytic and numerical problems.

Average values (Avg)

In each element Patch Ω^k , the Average values procedure for transferring element fields is splitted into three steps which are summarized in Fig. 1.

First the average values are projected from the old Gauss point g to the old nodes k . Such that an element patch Ω^k represents a union of elements containing the vertex node k , see Fig. 3.

$$\forall k \in \Omega_{old}^k, \tilde{\sigma}_k = \frac{1}{\sum_{el \in \Omega_{old}^k} \omega^{el}} \sum_{el \in \Omega_{old}^k} \omega^{el} \sigma_h^{el} \text{ such that} \\ : \omega^{el} = \sum_{g \in el} \omega^g, \quad (20)$$

where w^g and w^{el} are the volume contribution associated to Gauss point g and to element el , respectively.

Then, as mentioned in [7], the values at the new nodal points can be computed by simple interpolation of the old nodal values using the local interpolation functions such as the finite element shape function.

$$\forall k \in \Omega_{old}, \tilde{\sigma}_x = \sum_{k \in \Omega_{old}}^{nnt} \tilde{\sigma}_k N_{old}(\xi(x)), \quad (21)$$

where nnt is the total number of node in each element, $\xi(x)$ are the local coordinates of the new node x in the old mesh and N_{old} are the old FE shape functions used to interpolate the nodal variables.

Finally, the history dependent values at the integration points of the new mesh can be achieved by using local shape function of the new elements.

$$\forall x \in \Omega_{new}, \tilde{\sigma} = \sum_{x \in \Omega_{new}}^{nnt} \tilde{\sigma}_x N_{new}(\xi(g)), \quad (22)$$

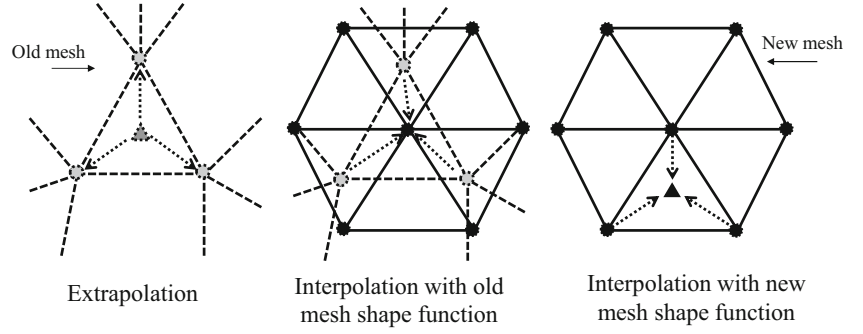
where $\xi(g)$ are the local coordinates of the new Gauss point in the new mesh and N_{new} are the new FE shape functions.

This method has the advantage of being applicable easily to any type of complex three-dimensional case by not having to consider the discretization of the two meshes involved. But its first extrapolation step constitutes an important source of numerical diffusion. In order to limit this diffusion, many other advanced techniques have also been proposed such as the Super-convergent Patch Recovery proposed by Zienkiewicz et Zhu [9–12].

Super-convergent patch recovery (SPR) technique

The FE approximation of a one-dimensional linear function can be locally very different from the exact solution, as shown in Fig. 2. However, at certain points in the elements, the results are nearly correct. These super-convergent points are located in the center of the elements which correspond to the element

Fig. 1 A tree-step procedure illustrating the indirect element field transfer



Gauss points. This prediction is proposed by Zienkiewicz and Zhu [9–12] and recommended by Babuska et al. [23] through numerical investigations.

To compute the recovered stress field $\tilde{\sigma}$ of each element (represented in Eq. (22)), the following expression is generally used for each patch. Such that an element patch Ω^k represents a union of elements containing the vertex node k , see Fig. 3:

$$\forall k \in \Omega_{old}^k, \tilde{\sigma} = \sum_{k=1}^{NG} \tilde{\sigma}_k N_k(x, y, z) = \sum_{k=1}^{NG} P \cdot a^k N_k(x, y, z) \quad (23)$$

The Eq. (23) is valid only over the old element patch Ω_{old} where NG is the total number of Gauss points in the patch, N_k the FE shape functions used to interpolate the nodal variables, $\tilde{\sigma}_k$ is the recovered solution at node k computed by considering a polynomial expansion P and a is a vector of unknown parameters. For a three-dimensional problem and for linear tetrahedral elements, we have:

$$P = (1, x, y, z) \quad (24)$$

$$a^k = (a_1^k, a_2^k, a_3^k, a_4^k)^t \quad (25)$$

The determination of the coefficients a_i^k for each component of the stress tensor consists of minimizing the following functional:

$$\begin{aligned} \pi(a^k) &= \sum_{i=1}^{NG} (\sigma_h(i) - \tilde{\sigma}(i))^2 \\ &= \sum_{i=1}^{NG} (\sigma_h(i) - P(x_i, y_i, z_i) \cdot a^k N_k(x, y, z))^2, \end{aligned} \quad (26)$$

where $\sigma_h(i)$ is the FE stress field calculated at coordinates (x_i, y_i, z_i) of Gauss point i .

The minimization problem is:

$$\forall i = 1..4, \frac{\partial \pi(a^k)}{\partial a_i^k} = 0 \quad (27)$$

Eq. (27) can be solved in matrix form as:

$$a^k = A^{-1}b, \quad (28)$$

where:

$$\begin{aligned} A &= \sum_{i=1}^{NG} P^t(x_i, y_i, z_i) P(x_i, y_i, z_i) \\ &= \sum_{i=1}^{NG} \begin{bmatrix} 1 & x_i & y_i & z_i \\ x_i & (x_i)^C & x_i y_i & x_i z_i \\ y_i & y_i x_i & (y_i)^C & y_i z_i \\ z_i & z_i x_i & z_i y_i & (z_i)^C \end{bmatrix} \end{aligned} \quad (29)$$

$$b = \sum_{i=1}^{NG} \sigma_h(i) P^t(x_i, y_i, z_i) = \sum_{i=1}^{NG} \sigma_h(i) \begin{bmatrix} 1 \\ x_i \\ y_i \\ z_i \end{bmatrix} \quad (30)$$

Finally, the elements smoothed stress distribution $\tilde{\sigma}$ is then computed at the node k (center of the patch) by inserting its coordinates in Eq. (23), where:

$$\tilde{\sigma}_k = P(x_k, y_k, z_k) a^k \quad (31)$$

The history dependent values at the integration points of the new mesh can be achieved by interpolating the obtained nodal recovered solution σ_k from old node to the new one using Eq. (21), then from old Gauss point to the new one using Eq. (22).

Particularly, the superconvergent patch recovery (SPR) technique is often preferred by several authors because it is robust and simple to use [18, 19]. However, for borders nodes Fig. 3, in the majority of cases the number of integration points is insufficient to determinate the coefficients of the polynomial expansion [9, 24]. In fact, the matrix A in Eq.

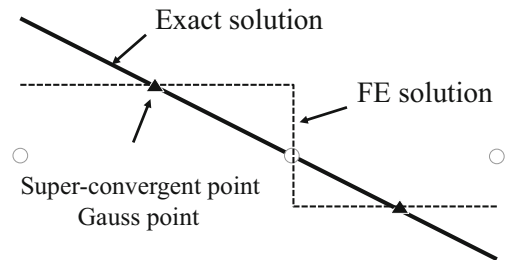
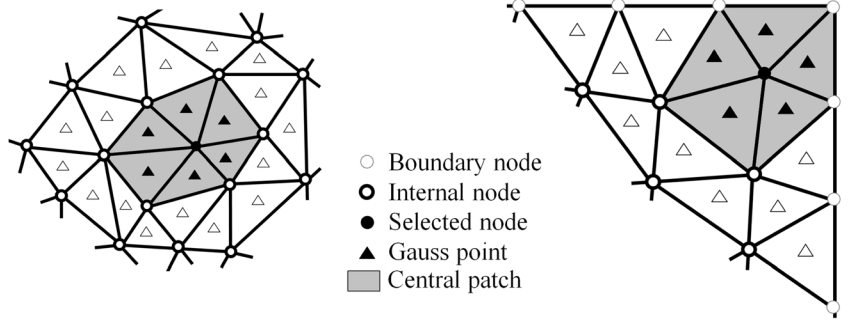


Fig. 2 Approximated values and exact solution

Fig. 3 Two-dimensional superconvergent patch recovery (SPR)



(29) is non-reversible. For a border node, Zienkiewicz and Zhu [9, 12] propose to calculate the value of $\tilde{\sigma}_k$ from a topological patch centered on an internal node closest to external node. Thus $\tilde{\sigma}_k^{ext}$ gets the neighbor value $\tilde{\sigma}_k^{int}$.

The Liszka-Orkisz variant of SPR (SPR-P)

In order to solve the boundary nodes problems the concept of the extended patch (see Fig. 4) introduced by Liszka-Orkisz' et al. [25, 26] can be used, where the nodal variables can be regarded as first (or second) order Taylor series expansion

over the extended topology P in the element patch Ω^k . For linear constraints, a Taylor series expansion to the first order of the FE stress at the Gauss points can be given as:

$$\forall k \in \Omega^k, \tilde{\sigma}_k = P(x_k, y_k, z_k) a^k \quad (32)$$

$$(1st\ order) = a_1^k + a_2^k(x-x_k) + a_3^k(y-y_k) + a_4^k(z-z_k) \quad (33)$$

Then, the minimization problem is:

$$\pi_k^{FD}(a^k) = \sum_{g \in \Omega^k} \left(\frac{\sigma_g - (a_1^k + a_2^k(x_g - x_k) + a_3^k(y_g - y_k) + a_4^k(z_g - z_k))}{\Delta r_g^2} \right)^2 = \sum_{g \in \Omega^k} \frac{O((\Delta r_g)^2)}{\Delta r_g^4} \quad (34)$$

with:

$$\Delta r_g^2 = (x^g - x^k)^2 + (y^g - y^k)^2 + (z^g - z^k)^2 \quad (35)$$

And similar to the standard form SPR the Eq. (34) can be solved in matrix form as:

$$a^k = A^{-1}b, \quad (36)$$

where:

$$A = \sum_{g=1}^{NG} \frac{1}{\Delta r_g^4} P^t(x_g, y_g, z_g) P(x_g, y_g, z_g) \\ = \sum_{g=1}^{NG} \frac{1}{\Delta r_g^4} \begin{bmatrix} 1 & \Delta x_g & \Delta y_g & \Delta z_g \\ \Delta x_g & (\Delta x_g)^c & \Delta x_g \Delta y_g & \Delta x_g \Delta z_g \\ \Delta y_g & \Delta y_g \Delta x_g & (\Delta y_g)^c & \Delta y_g \Delta z_g \\ \Delta z_g & \Delta z_g \Delta x_g & \Delta z_g \Delta y_g & (\Delta z_g)^c \end{bmatrix} \quad (37)$$

$$b = \sum_{g=1}^{NG} \sigma_h(g) P^t(x_g, y_g, z_g) = \sum_{g=1}^{NG} \sigma_h(g) \begin{bmatrix} 1 \\ \Delta x_g \\ \Delta y_g \\ \Delta z_g \end{bmatrix}, \quad (38)$$

with:

$$\Delta x_g = x^g - x^k; \Delta y_g = y^g - y^k; \Delta z_g = z^g - z^k \quad (39)$$

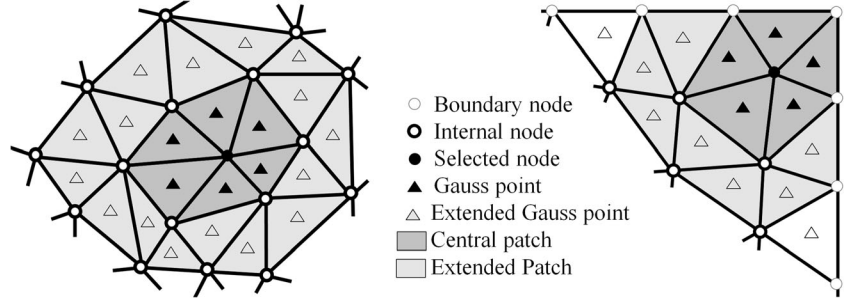
The weighting term $\frac{1}{\Delta r_g^4}$ allows to varying the weight of the contributions of neighbors in the patch. This weight is even important if the corresponding Gauss Point g is closer to the central node k of the patch. However in the SPR technique all the neighbors have the same weight.

Analytical results

Efficiency of the adaptive remeshing strategies

In this section, an analytical function $f_1(x, y, z)$ is used to check the sensitivity of the described a posteriori error estimation (section: Size map for adaptive strategies) for detecting the presence of significant error localization and to test the capabilities of the presented adaptive remeshing strategies (section: Patch Recovery

Fig. 4 Two-dimensional superconvergent extended patch recovery (SPR-P)



Techniques) in the presence of various levels of pollution error (Fig. 5).

$$f_1(x, y, z) = 100^* \sqrt{\tanh\left(3(x-0,3)^{7*}(y-0,3)^{7*}(z-1,3)^5 + 1\right)} \quad (40)$$

$$\begin{cases} x : [-1..1] \\ y : [-1..1] \\ z : [-1..1] \end{cases}$$

The adaptive procedure starts approximately with 21,000 uniformly distributed elements. A target error $\tilde{\theta}_{el}^{opt}$ in the adaptive process of 0.8% was adopted. The results are shown in Fig. 6, where each line corresponds to a remeshing step taking the mesh in the previous line as the initial mesh. In practice, the elements size can't respect perfectly the target error; hence, the sizes of elements can be very small or very large, especially in the high gradient zones. The main cause of this non respect is the obligation to insert a midcap mesh in these zones in order to create a better evolution of the mesh size map. To evaluate the efficiency of the different used processes, global and local checks can be used: a first check is undertaken to simply calculate the average error of the new discretization. If this error is not close to the desired precision, it is certain that the built mesh is not optimal. However, even if the overall error is close to the desired one, this does not prove the optimality of new mesh. The main idea of the local check is to verify the error of the entire domain Ω for each element. In fact, if the element size is optimal, the procedure of successive adaptation must give change coefficients close to 1. According to [17], the size of the elements is considered satisfying in all areas with his modification size coefficient R^e , where we have:

$$2/3 \leq R^e \leq 3/2, R^e = h^{new}/h^{old}, \quad (41)$$

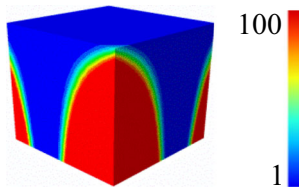


Fig. 5 The analytic values of the function $f_1(x,y,z)$

As shown in Fig. 6, after each remeshing steps the density of element will increase or decrease in some zones in order to respect the target error. The evolution of the number of element in the histograms plot showed a concentration rise of elements numbers around the target error after each meshing step. For this analytic function five iterations can be considered as satisfactory because the modification coefficients of element size R^e is 90%, close to 1 in overall domain. In there-after examples this coefficients of element size criteria will be used in order to define the ideal number of iteration for each FEM problem.

Selection of the best recovery techniques

In order to select the best Patch Recovery Techniques to transfer the data state variables between two meshes, several analytical functions (linear and nonlinear) are considered in Fig. 7. Here, we measure the exact error value, since the true solution is known. The approximated solution is made by using the smoothing techniques. The accuracy and convergence of each technique is examined with two different L2 error norms which are volumetric norm Eq. (42) and surface norm Eq. (43). These L2 error norms measure the error between the recovered field values and the exact analytic solution.

$$\|\xi\|_{vol} = \sqrt{\frac{\sum_k |f_k(analy) - f_k(SPR/SPR_P/Avg)|^2}{\sum_k |f_k(analy)|^2}}; \forall k \in \Omega \quad (42)$$

$$\|\xi\|_{surf} = \sqrt{\frac{\sum_k |f_k(analy) - f_k(SPR/SPR_P/Avg)|^2}{\sum_k |f_k(analy)|^2}}; \forall k \in \partial\Omega \quad (43)$$

Figure 7 presents the volume and surface error values for SPR, SPR-P and Average recovery operator obtained for linear, quadratic, trigonometric and exponential functions for several meshes with uniformly decreasing element sizes. The corresponding comparison shows how the SPR technique values represent an improvement with respect to

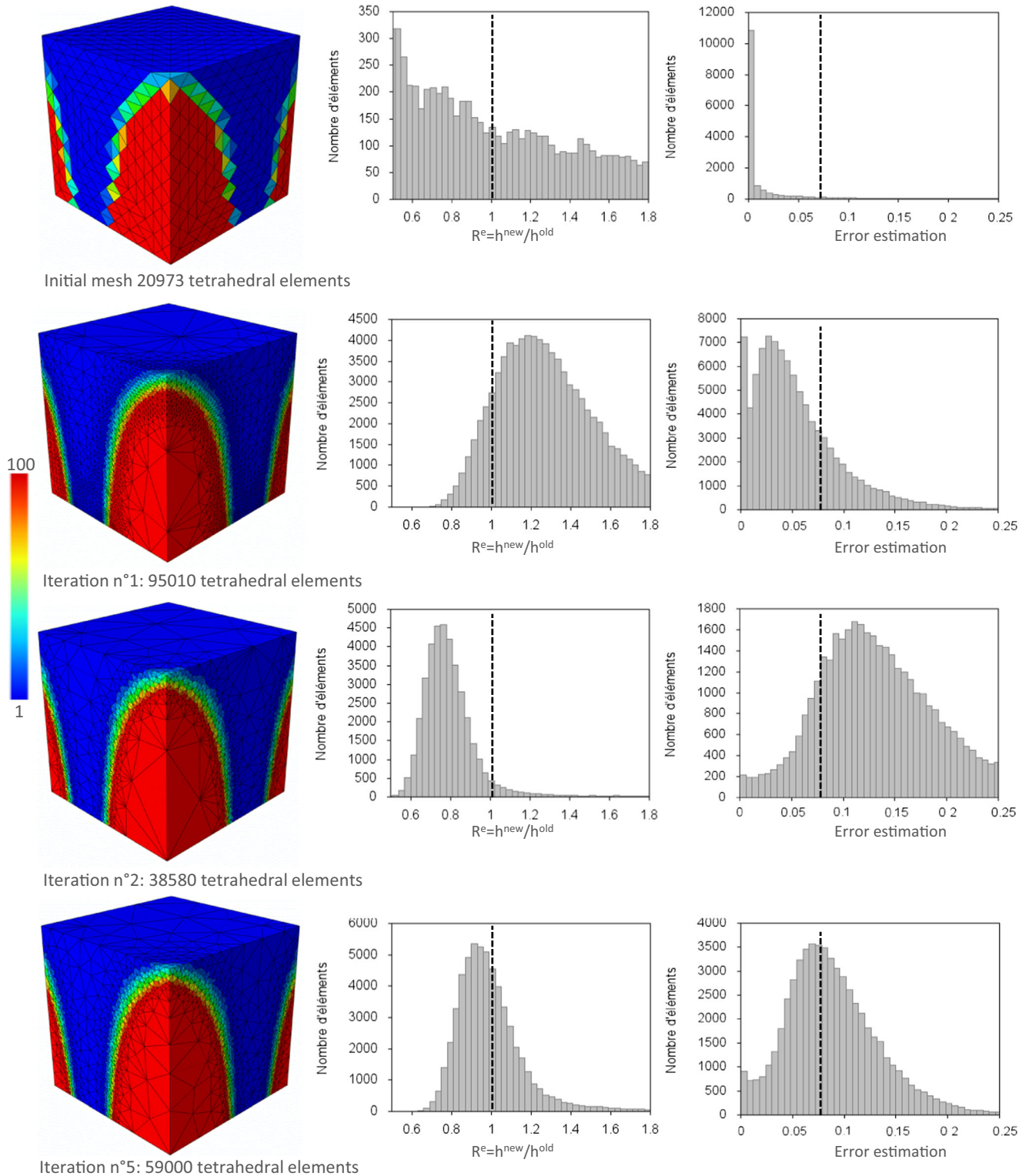


Fig. 6 Iso values of the tested analytical function: $f_1(x,y,z)$ mesh size coefficient: R^e , and local error estimation for each remeshing step

the analytic values inside the domain, in comparison with the other techniques; but this improvement is not enough to ensure a good surface error prediction. This verdict is well known when the standard SPR technique is applied to boundary points, especially for coarse meshes. In order to

reduce the surface error booth, SPR-P and Average recovery technique can be used. Also, we can note that the error estimation both on surface and inside the domain illustrates better results with SPR-P recovery compared to the Average recovery technique.

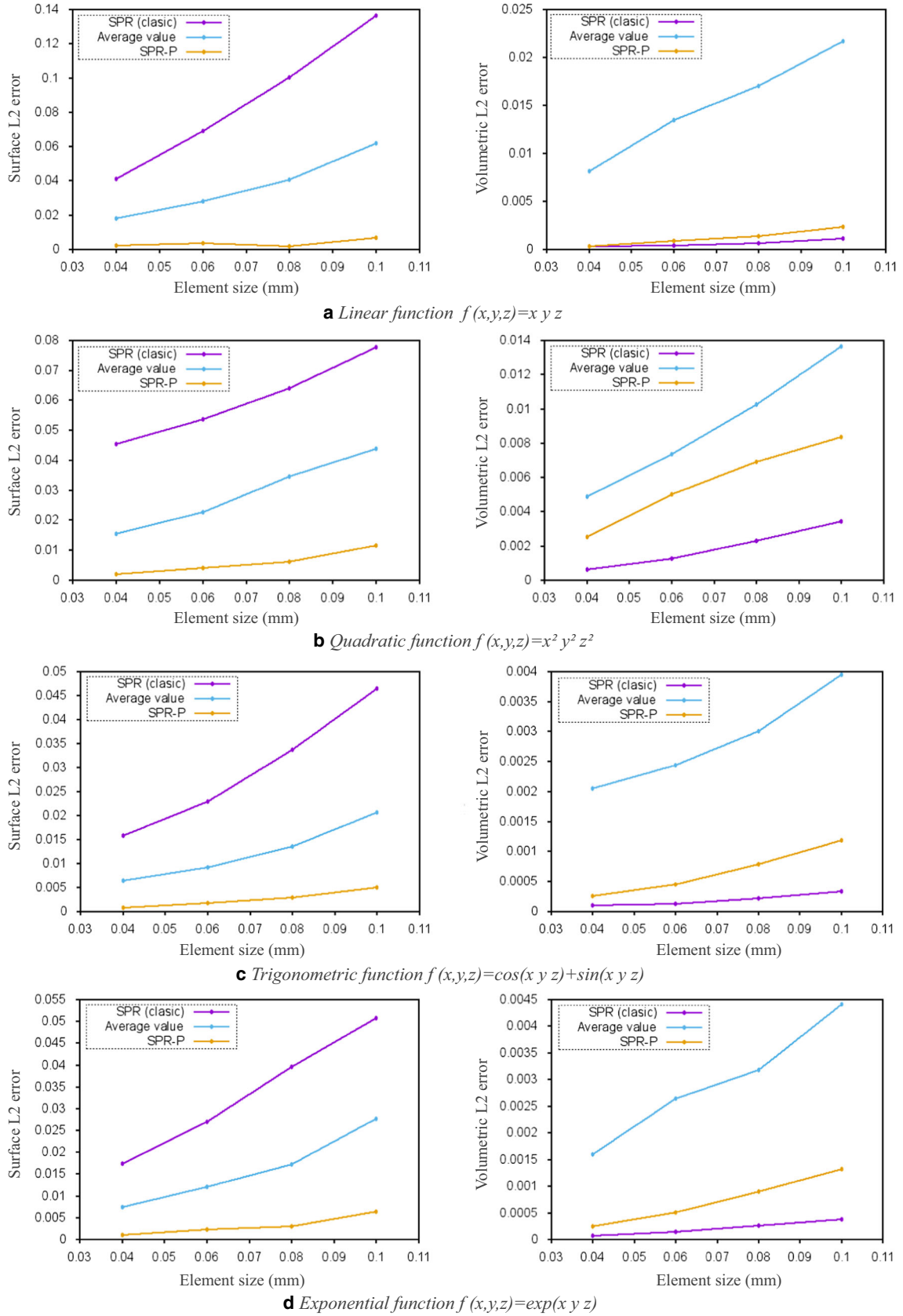


Fig. 7 Comparison between some indirect transfer operators with linear, quadratic, trigonometric and exponential functions

For this work and in order to combine the advantage of these methods the SPR technique will be used to transfer the variables inside the domain and the SPR-P technique will be used to transfer the surface ones.

Adaptive REMESHING methodology

The proposed automatic adaptive remeshing strategy is presented in Fig. 8 and tested by solving two numerical examples under large inelastic deformations and high strain localization. The purpose of these examples is to illustrate the efficiency of the adaptive remeshing scheme adopted to optimize the mesh according to the aimed prediction and to improve a good quality of elements in each step-time. In this work and similar to [7], an element is classified as being distorted if one of his dihedral angles (angles between two faces) is larger than 160° or smaller than 10° , or if the radius-element ratio (the ratio between the volume of initial tetrahedron and the volume of

the regular tetrahedron registered in the same circumscribed ball, Fig. 9) is smaller than 0.2.

Only for the first step, the initial finite elements discretization using a tetrahedral element is provided. Then, for each time step an ABAQUS 6.13/ Explicit FE calculation is performed with a small test displacement, and the resulting simulation is analyzed through a posteriori error estimators and element quality. If the estimated elementary error and / or the number of distorted elements does not exceed a given threshold, the previous FE simulation will be continued. Else, the mesh is then modified automatically (refined and / or coarsened) with MeshGems software according to the constantly changing physical fields and geometrical shape and a new solution for this loading sequence is computed. For each time step, this process is repeated many times until the mesh no longer changes and/or the error level has been reached. Finally, all field variables are transferred from the old mesh to the new one and the simulation is restarted from the previous time step. It should also be noted that after each time step,

Fig. 8 Flow chart of the FE-simulation for 3D remeshing module

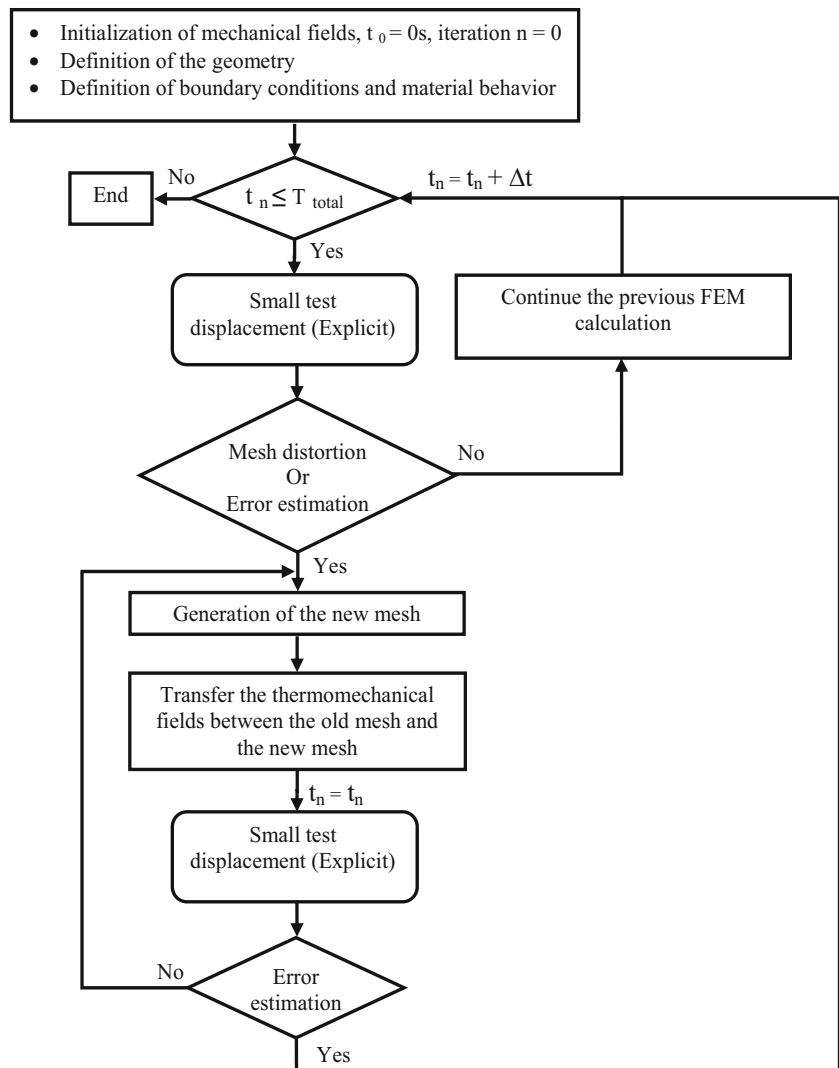
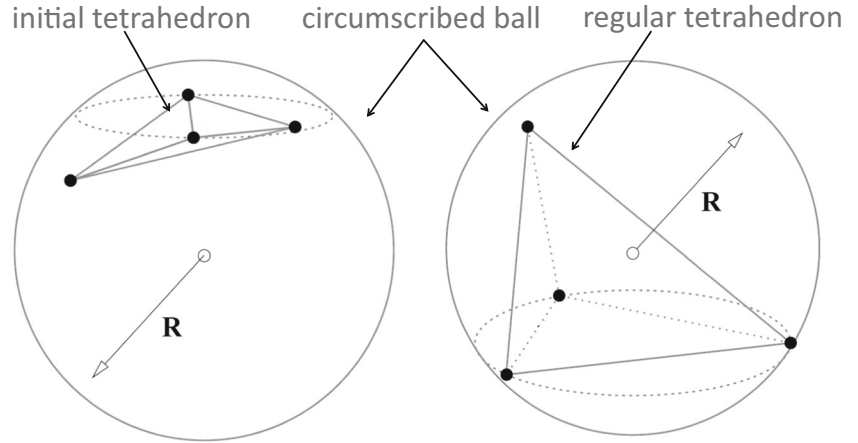


Fig. 9 The radius-volume ratio of tetrahedron



the boundary and loading conditions are generated according to the old step modification.

Numerical results

Shear test

First, a shear test is used in order to validate the proposed methodology and study some numerical aspects. Then, a metal forming process of a complex geometry will be tested. In each case, both the tool and the workpiece are discretized with tetrahedral elements C3D4T with thermomechanical coupling taken from ABAQUS element library. The mesh of the tools is selected before the first step and remains unchanged. However, the initial mesh of the work piece is a regular coarse mesh and will be automatically adapted during the FE process. In the adaptive process the smallest h_{min} and largest h_{max} element sizes are respectively 0.1 mm and 1 mm. The contact interface between the tools and the parts is modelled by the classical Coulomb model with a constant friction coefficient

$\eta = 0.2$. Finally, material subroutine Vumat is implemented to predict the Johnson-Cook model [27] at each Gauss point for titanium alloy Ti17. The mechanical properties are similar to those reported in Reference [28].

For the shear test, the geometry dimensions and boundary conditions are given in Fig. 10. According to the symmetry conditions in a 3D configuration, only one quarter of the workpiece is modeled. To illustrate the efficiency of the adaptive strategy under large inelastic deformations and high strain localization, two uniform displacements of the rigid tool has been analyzed. All the adaptive procedure starts with 2493 uniformly distributed elements (Fig. 11a). Also, in order to attend the convergence of the FE solution and to study the influence of the element size on the stability of load, three target errors of 1%, 0.1%, and 0.03% have been used in the adaptive process. In this adaptive process, the smallest h_{min} and largest h_{max} element sizes are 0.1 mm and 1 mm respectively.

Fig. 11b shows the final mesh obtained after four adaptive remeshing loops that can be compared with the initial one Fig. 11a. This adaptive remeshing loop is adopted at every time

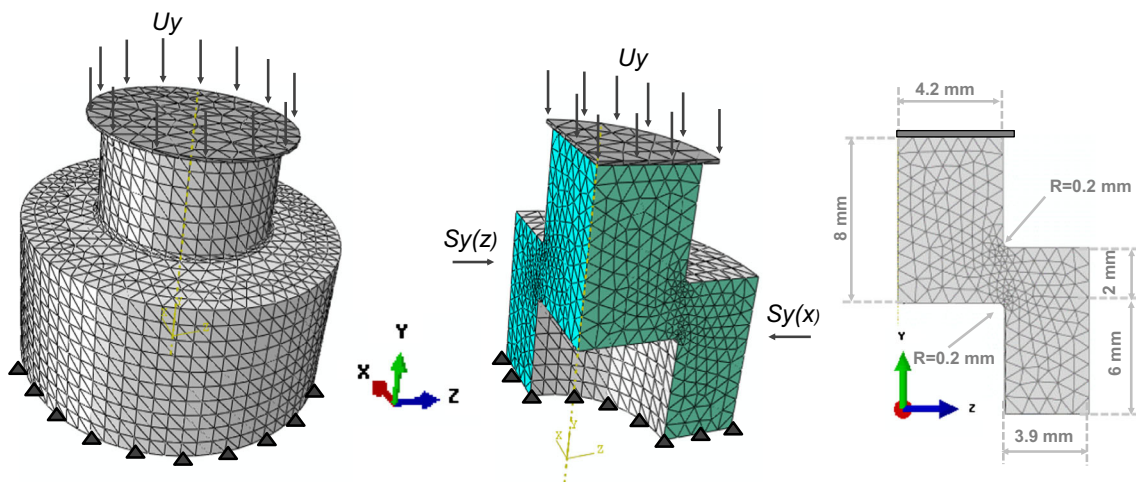
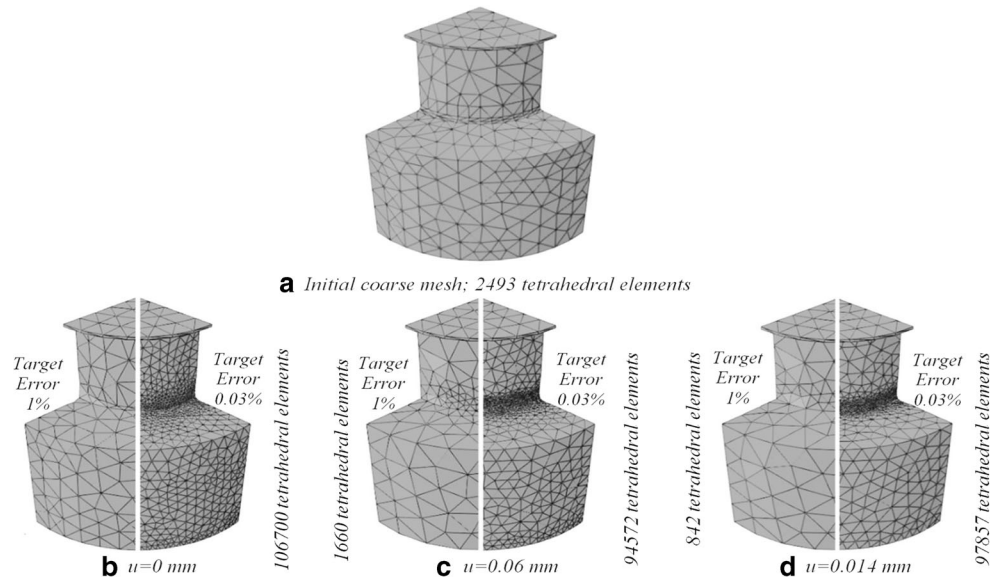


Fig. 10 Geometry and boundary conditions of the specimens used in shear test

Fig. 11 Meshes at different instants with different targets errors



step taking the adaptive deformed mesh in the previous step as the initial mesh. It can be observed how the adapted mesh concentrates additional elements in the critical zones whereas the number of elements in the rest of the domain remains practically unaltered or decreased.

We can note that the element size increases and the number of elements decreases with increasing the imposed target error.

The comparison between the numerical load–displacement curves and published experimental data [28] with different deformation rate 1 mm/s and 100 mm/s are shown in Fig. 12. At Fig. 12a, it can be shown that the smallest target error 0.03% is much more efficient in terms of convergence and accuracy of the FE solution in comparison with the large values 0.1 and 1%. However, even with this small target error 0.03% the system is not in mechanical equilibrium anymore. In fact, the numerical curves show a small fluctuation in the load-displacement response after each remeshing step which can be caused by a small degree of numerical diffusion during the transfer of variables between subsequent meshes. Also, we

can note that the level of fluctuation decreases with the decrease of the target error used in the adaptive process. This non-smooth pattern fluctuation is also observed using various others approaches such as average values, closest point technique [7], Superconvergent Patch Recovery (SPR) [22] or the unique element method (UEM) [29].

In Fig. 12b, we consider the same shear test as previously presented in Fig. 12a, but the shear test is performed under a high deformation rate of 100 mm/s. More fluctuation of load–displacement curves results under high deformation rate in comparison to the low one are observed.

Equilibrium process

In order to solve the problem of this numerical instability, the results obtained before and after data transfer process between two successive meshes are compared. In Fig. 13, the first line and the second one show the distribution of the von Mises stress components at integration points in each element; the

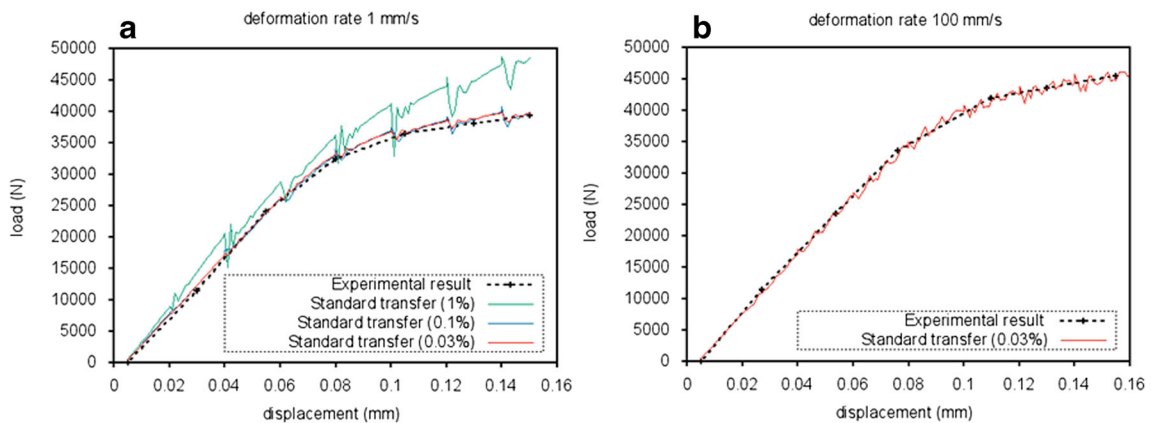
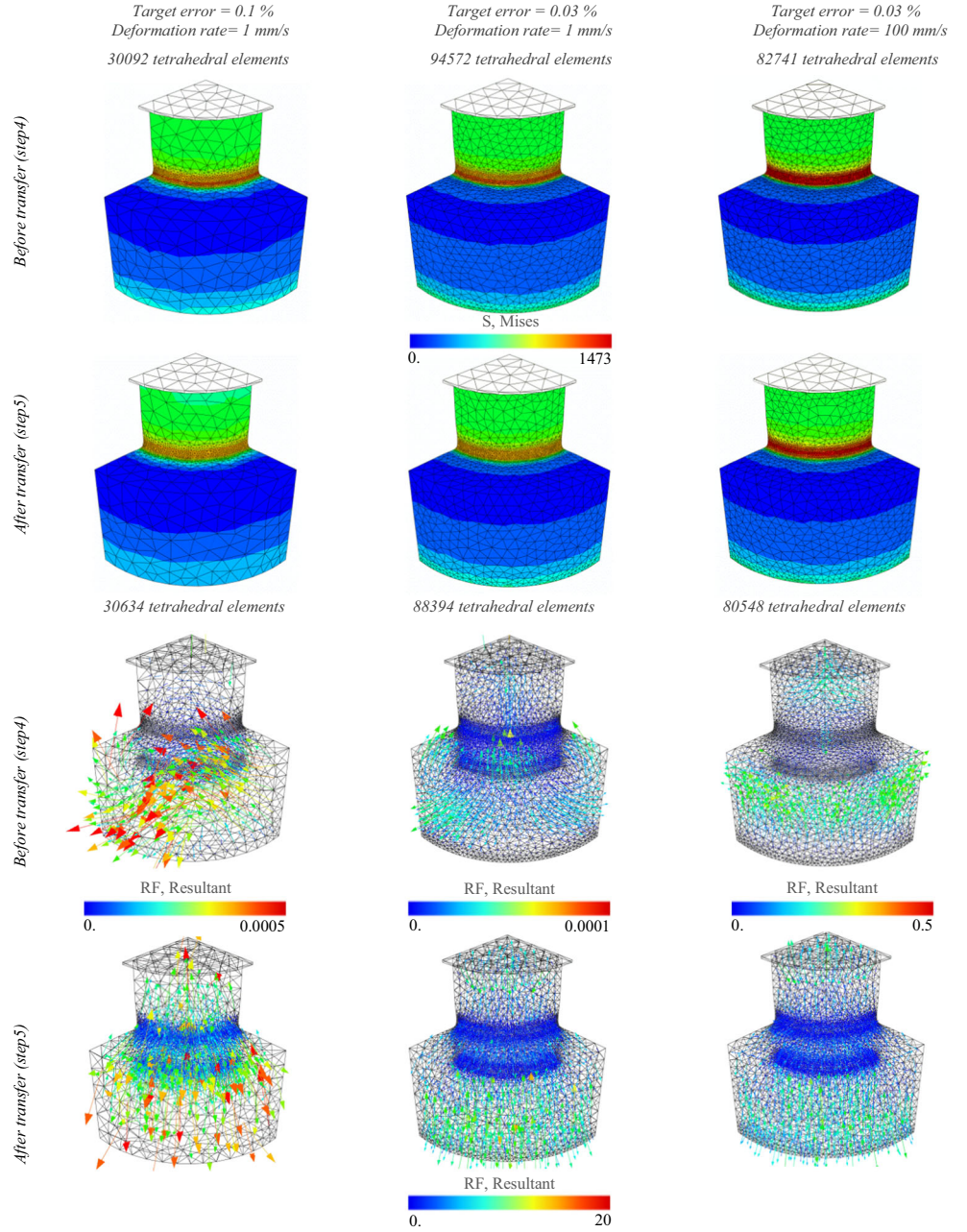


Fig. 12 Comparison of load–displacement curves of mechanical tests using different deformation rate: 1 mm/s and 100 mm/s

Fig. 13 The evolution of the von Mises stress and the nodal force caused by stress smoothing before and after transfer at the same displacement $u = 0.08$ mm



third line and the fourth one show the value of internal forces at tetrahedral element nodes Eq. (44).

$$f^{int} = \begin{bmatrix} f_{x_1}^{int} \\ f_{y_1}^{int} \\ f_{z_1}^{int} \\ \vdots \\ f_{x_{nnt}}^{int} \\ f_{y_{nnt}}^{int} \\ f_{z_{nnt}}^{int} \end{bmatrix} = \int_V B^T \tilde{\sigma} dV, \quad (44)$$

where B is the spatial derivatives of the FE shape function.

The second line in Fig. 13 show a good continuous evolution of the von Mises stress after the transfer, due to the stress smoothing. However, only with small target error test, very small smooth diffusion can be seen. Before meshing, the nodal forces in the old mesh are very small since the explicit solver is used as shown in the third line and Eq. (45). However, it is not the case after remeshing specially in highly stain regions as shown in the fourth line. At this stage the main cause of the unbalanced system is due to the non-equilibrated forces at element nodes caused by stress smoothing in element. These nodal forces were self-equilibrated before transfer of state variables because the previous converged state was

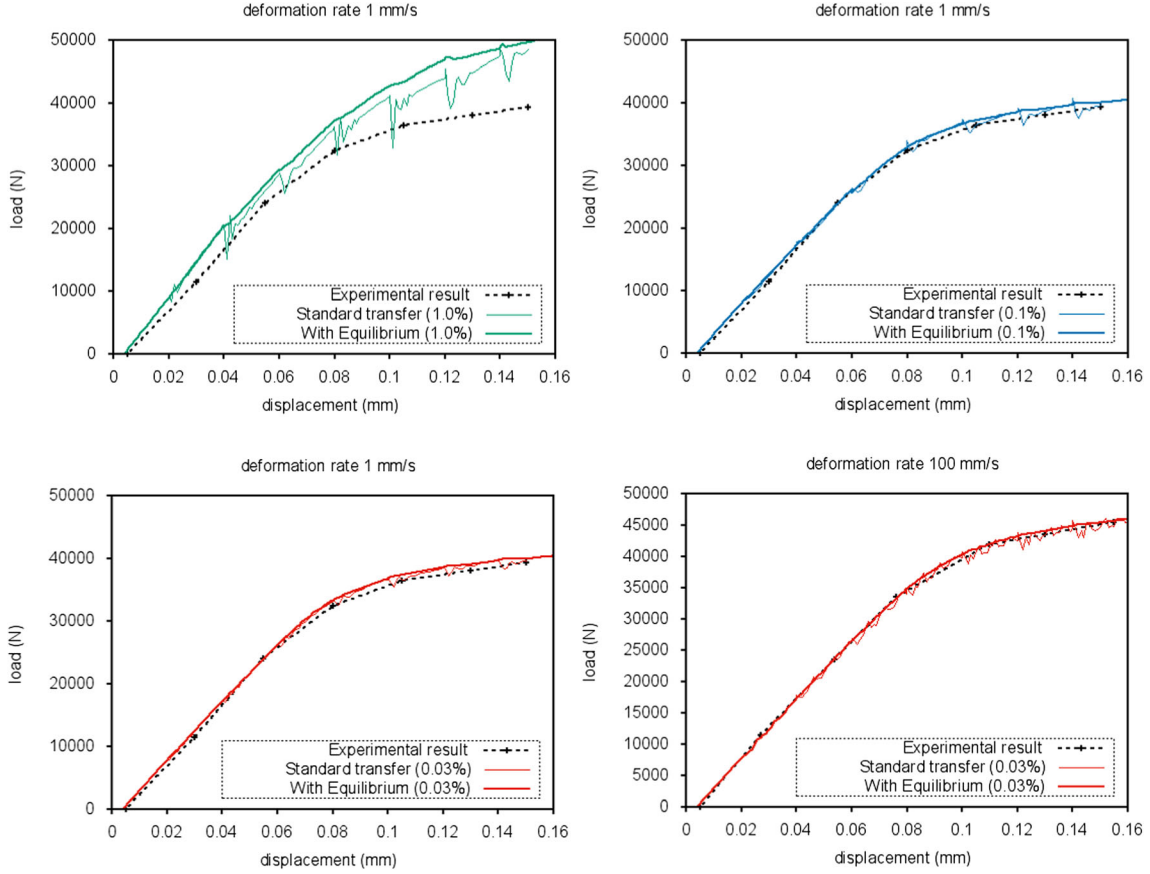


Fig. 14 Comparison of load–displacement curves of mechanical tests before and after equilibrium

valid only for the old mesh Eq. (45), but became external forces after transfer and are no longer in self-equilibrium with the new dynamic equilibrium equations Eq. (46).

$$\text{div}(\sigma_{old}^{el}) - m_{old}^n \cdot \gamma_{old}^n = 0 \quad (45)$$

$$\text{div}(\sigma_{new}^{el}) - m_{new}^n \cdot \gamma_{new}^n \neq 0, \quad (46)$$

where σ_{old}^{el} and σ_{new}^{el} are respectively the initial and transferred stress. $(m_{old}^n \cdot \gamma_{old}^n)$ and $(m_{new}^n \cdot \gamma_{new}^n)$ are respectively the mass and acceleration of each node of the initial and finally mesh. From Figs. 12 and 13, it can be construed that if the rate deformation or the elements size used during the numeric simulation is sufficiently small, mechanical equilibrium can be established again at small time increment, because the transfer error is too small. In the case of high rate deformation, the remeshing process cannot be used because the numerical instability will be amplified (third row in Fig. 13) even if the transfer error is too small.

So, to restore equilibrium with the new boundary conditions the unbalanced internal forces must be removed. However, if they are eliminated at once, often the following iterations are found in mechanical imbalance, especially for coarse meshes. Analogy example of Spring-mass system can be helpful to solve the equilibrium problem. In fact, when a

spring is stretched or compressed by a mass, the spring develops a restoring force. Only if this restoring force is small or relaxed the Spring-mass system can easily reach back to equilibrium. From this idea, a relaxation procedure has been implemented during the next step where these unbalanced nodal forces are removed successively by series of analytic function

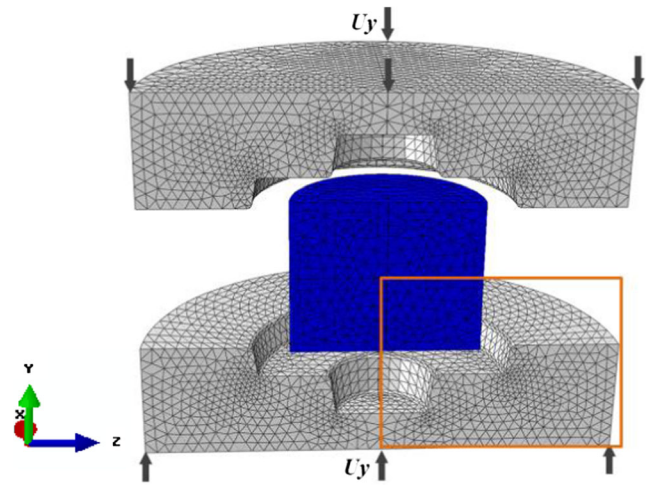


Fig. 15 Geometry, boundary conditions, and initial finite elements discretization

with decreasing coefficients. Note that only the values of dynamic nodal force $m_{new}^n \cdot \gamma_{new}^n$ are kept. Where m_{new}^n is the nodal

mass of the new mesh discretization and the new acceleration values at the nodal points γ_{new}^n are computed by an

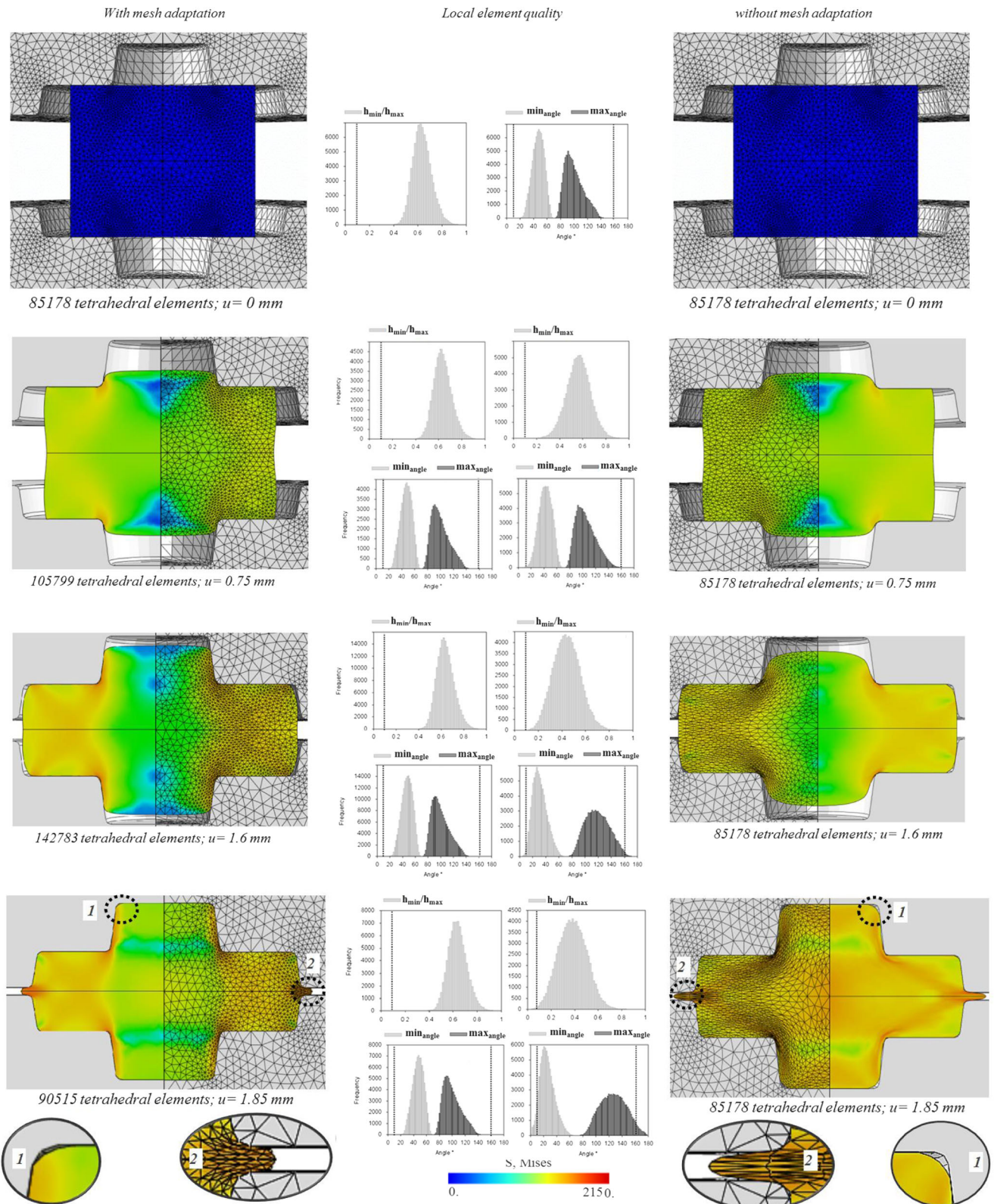


Fig. 16 Meshes at different tool displacement in the left with mesh adaptation and in the right without mesh adaptation

interpolation of the old nodal acceleration via the FE shape function. The obtained results are presented in Fig. 14.

It is obvious in Fig. 14 that the equilibrium recovery proposed in this work allows to restore equilibrium after each meshing step. In terms of convergence under high and low rate deformation, the computed load/displacement responses obtained with equilibrium process give a good approximation of the experimental solution compared to the one obtained by only direct transfer.

From these results, it can be concluded that the use of adaptive mesh process coupled with the proposed equilibrium recovery has the better results compared to the use of standard one, for which the equilibrium recovery process is not imposed.

Metal forming processes

The metal forging is simulated with Abaqus 6.13 software. The half of geometry and boundary conditions are shown in Fig. 15. According to the symmetry conditions, only an eighth workpiece is modeled.

In order to demonstrate the interest and efficiency of adaptive remeshing at a more complex geometries level, the same metal forging simulation is carried out with the presented mesh adaptation strategy (adaptive case) and without mesh adaptation (standard case). One of the critical ingredients in any FEM process is the mesh discretization. In fact, a severe mesh distortion can occur during the standard simulation especially with constant coarse mesh. However, it is not the case with the adaptive test because the mesh is automatically adapted according to the constant change (physical fields and geometrical shapes). That's why the initial mesh of the standard test must be optimized in some critical zones as shown in Fig. 16. This comparison can improve a first advantage of using the adaptive process to avoid excessive mesh refinement, and present a good filling of the die matrices.

The numerical results presented in Fig. 16 show the efficiency of the adaptive remeshing process. In fact, from the beginning of the simulation to the end, a good quality of elements is proved with the adaptive strategy. However, a severe mesh distortion is observed without mesh adaptation. With the adaptive process, the simulation ends with zero element distortion compared to 6325 distorted elements without remeshing.

As it was noted above, each element size can be considered as optimal only if the procedures of successive mesh adaptation give modification coefficient are close to 1. So, the remeshing iteration is repeated many times until the total number of optimal elements does not exceed a given threshold. For this metal forging simulation, the target threshold of optimal elements number is selected as 75% and more strict area of modification coefficient is chosen $3/4 \leq R^e \leq 5/4$ compared to the reference coefficient proposed by Ladevèze [17] which is

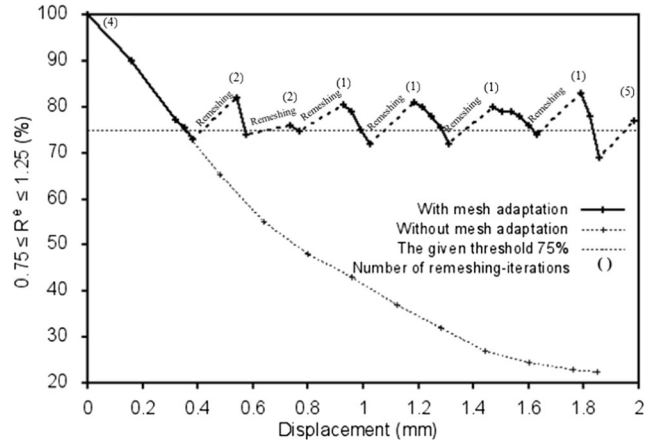


Fig. 17 The evolution of the percentage of optimal element with and without mesh adaptation

$2/3 \leq R^e \leq 3/2$ Fig. 17 shows that the both simulations start with the same number of optimal elements. With the standard process, the percentage of optimal element decrease after each load displacement step until the end of simulation. In this stage, only 23% of elements are conformed to the target error. However, with the adaptive process if the percentage of optimal element is above the given threshold 75%, the previous FE simulation will be continued. Else, the mesh is then modified automatically according to the constant change of physical fields and geometrical shape. Another strong point of the presented process is that for each time step, the number of remeshing-iterations is not fixed, but it is automatically adapted, as shown in Fig. 17. This characteristic can avoid the useless iteration and reduce time cost. For example for the first meshing step four iterations are performed; for the second and third meshing step two iterations; for the fourth meshing step only one iteration is used.

The evolution of numerical load–displacement curves with and without adaptive remeshing is compared in Fig. 18. At the beginning of simulation both EF simulations give similar results. However, it is not the case at the end of test. This

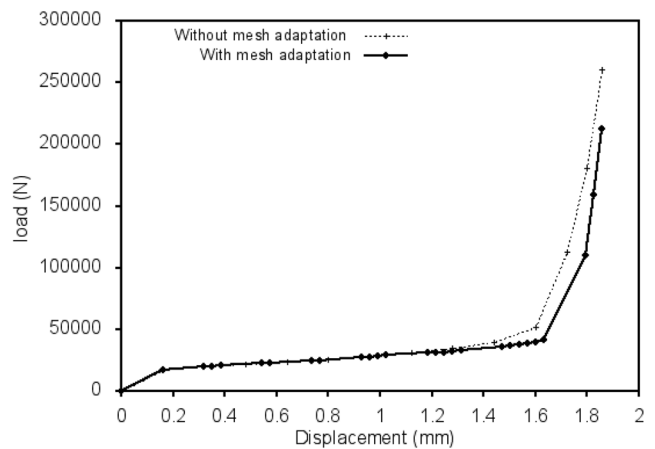


Fig. 18 Comparison of load–displacement curves of forming tests with and without mesh adaptation

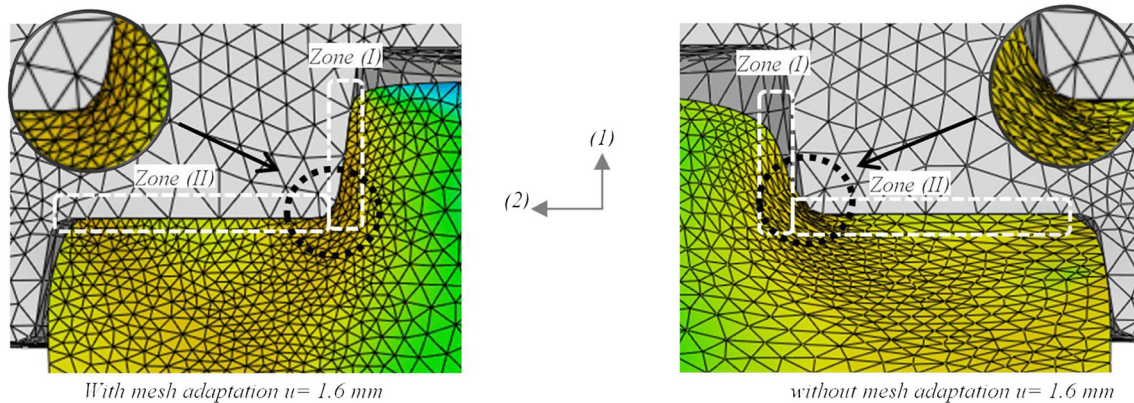


Fig. 19 The effect of mesh-distortion on the geometry of the workpiece

difference may be caused by the presence of excessive mesh distortion in the standard test (without adaptive remeshing). As can be seen in Figs. 16 and 19, these mesh distortions favors the displacement of elements in the second direction compared to the first one. In other words, the contact area between the rigid tool and the workpiece will not be the same especially in the second zone (II), which have a strongly effect on the normal load.

Conclusion

In this paper, an automatic adaptive remeshing method based on local mesh modification has been presented to simulate various 3D metal forming processes in large elastoplastic deformations. This process has been implemented with a small test displacement step by step in order to adapt automatically to the constantly changing physical fields and geometrical shapes. At each time-step, the remeshing iteration is repeated many times until the total number of optimal elements does not exceed a given threshold. This characteristic can avoid the useless iteration and reduce time cost. To avoid numerical diffusion during the mapping of variables, data transfer error is examined using analytical functions such as linear, quadratic, trigonometric and exponential with volumetric L2 error norms and surface one. The results show that these techniques illustrate different efficiency. So, in order to combine the advantage of these methods the SPR technique will be used to transfer the variables inside the domain and the SPR-P technique will be used to transfer the surface ones. Without equilibrate process, the numerical load-displacement curves under large displacement and/or high deformation rate show that after each remeshing step the system is not in mechanical equilibrium anymore. In fact, the numerical curves show a small fluctuation in the load-displacement response after each remeshing step. But with the proposed equilibrated process a good agreement with experimental data has been observed and the imbalance fluctuations are reduced significantly.

Also, a good quality of elements is proven with the adaptive strategy, where a severe mesh distortion is observed without mesh adaptation which can significantly reduce the efficiency of numerical result. Finally, the overall results are very encouraging and show the efficiency and robustness of the proposed strategy to avoid mesh distortion and to simulate more complex geometry levels with a better filling of the die matrices compared to the standard approach. However, several points can be improved such as damage evolution.

References

1. Diez P, Calderon G (2007) Remeshing criteria and proper error representations for goal oriented h-adaptivity. *Comput Methods Appl Mech Engrg* 196(4-6):719–733
2. Ainsworth M, Oden JT (1997) A posteriori error estimation in finite element analysis. *Comput Methods Appl Mech Engrg* 142(1-2):1–88
3. Verfurth R (1999) A review of a posteriori error estimation techniques for elasticity problems. *Comput Methods Appl Mech Engrg* 176(1-4):419–440
4. Lo SH (1991) Volume discretization into tetrahedra-I. Verification and orientation of boundary surfaces. *Comput Struct* 39(5):493–500
5. Lo SH (1991) Volume discretization into tetrahedra-II. 3D triangulation by advancing front approach. *Comput Struct* 39(5):501–511
6. Dureisseix D, Bavestrello H (2006) Information transfer between incompatible finite element meshes: application to coupled thermo-viscoelasticity. *Comput Methods Appl Mech Engrg* 85:6523–6541
7. Zeramdini B, Robert C, Germain G, Pottier T (2016) Simulation of metal forming processes with a 3D adaptive remeshing procedure. *AIP Conf Proceed*. <https://doi.org/10.1063/1.4963636>
8. Srikanth A, Zabarar N (2000) Shape optimization and preform design in metal forming processes. *Comput Methods Appl Mech Engrg* 190(13-14):1859–1901
9. Kumar S, Fourment L, Guerdoux S (2015) Parallel, second-order and consistent remeshing transfer operators for evolving meshes

- with superconvergence property on surface and volume. *Finite Elem Anal Des* 93:70–84
10. Peric D, Hochard C, Dutko M, Owen DRJ (1996) Transfer operators for evolving meshes in small strain elasto-plasticity. *Comput Methods Appl Mech Engrg* 137(3-4):331–344
 11. Zienkiewicz OC, Zhu JZ (1992) The superconvergent patch recovery (SPR) and adaptive finite element. *Comput Methods Appl Mech Engrg* 101(1-3):207–224
 12. Zienkiewicz OC, Zhu JZ (1992) The superconvergent patch recovery and a posteriori error estimation. Part I: the recovery technique. *Internat J Numer Methods Engrg* 33(7):1331–1364
 13. Zienkiewicz OC, Zhu JZ (1992) The superconvergent patch recovery and a posteriori error estimation. Part II: error estimates and adaptivity. *Internat J Numer Methods Engrg* 33(7):1365–1382
 14. Babuška I, Rheinboldt WC (1978) A posteriori error estimates for the finite element method. *Internat J Numer Methods Engrg* 12(10):1597–1615
 15. Ladevèze P, Coffignal G, Pelle J.P (1986) Accuracy of elastoplastic and dynamic analysis. In Babuška I, Zienkiewicz O.C, Gago J and Oliveira E.R de A, ch.11 Accuracy Estimates and Adaptive Refinements in Finite Element Computations, John Wiley & Sons Ltd pp 181–203
 16. Zienkiewicz OC, Zhu JZ (1987) A simple error estimator and adaptive procedure for practical engineering analysis. *Int J Numer Methods Eng* 24(2):337–357
 17. Ladevèze P, Pelle J.P (2004) Mastering calculation in linear and nonlinear mechanics, Berlin
 18. Boussetta R, Fourment L (2004) A posteriori error estimation and three-dimensional adaptive remeshing: application to error control of non-steady metal forming simulations. *AIP Conf Proc* 712: 2246–2251
 19. Boussetta R, Coupez T, Fourment L (2006) Adaptive remeshing based on a posteriori error estimation for forging simulation. *Comput Methods Appl Mech Engrg* 195(48-49):6626–6645
 20. Coorevits P, Bellenger E (2004) Alternative mesh optimality criteria for h-adaptive finite element method. *Finite Elem Anal Des* 40: 2195–2215
 21. Ciarlet P.G (1978) *The finite element method for elliptic problems*. North-Holland publishing company, Amsterdam, New York, 45, 4
 22. Khoei AR, Gharehbaghi SA, Tabarraie AR, Riahi A (2007) Error estimation, adaptivity and data transfer in enriched plasticity continua to analysis of shear band localization. *Appl Math Model* 31(6):983–1000
 23. Babuška I, Strouboulis T, Upadhyay CS, Gangaraj SK, Copps K (1994) Validation of a posteriori error estimators by numerical approach. *Int J Numer Methods Engrg* 37(7):1073–1123
 24. Wiberg NE, Abdulwahab F, Ziukas S (1994) Enhanced superconvergent patch recovery incorporating equilibrium and boundary conditions. *Inter J for Numer Methods Engrg* 37(20): 3417–3440
 25. Liszka T, Orkisz J (1980) The finite differences method at arbitrary irregular grids and its application in applied mechanics. *Comput Struct* 11(1-2):83–95
 26. Liszka T (1984) An interpolation method for an irregular net of nodes. *Int J Numer Methods Engrg* 20(9):1599–1612
 27. Johnson G.R, Cook W.K (1983) A constitutive model and data for metals subjected to large strains high strain rates and high temperatures. 7th international symposium on Ballistics pp 541–547
 28. Ayed Y, Germain G, Ammar A, Furet B (2016) Thermo-mechanical characterization of the Ti17 titanium alloy under extreme loading conditions. *Int J Adv Manuf Technol* 90:5–8. <https://doi.org/10.1007/s00170-016-9476-5>
 29. Hu Y, Randolph MF (1998) H-adaptive FE analysis of elasto-plastic non-homogeneous soil with large deformation. *Comput Geotech* 23(1-2):61–83